



OPEN ACCESS

EDITED BY

Sheng Guo,
Chalmers University of Technology,
Sweden

REVIEWED BY

Liulu Han,
Max-Planck-Institut für Eisenforschung,
Germany
Patrick Conway,
Jönköping University, Sweden

*CORRESPONDENCE

Weihong Liu,
✉ liuweihong@hit.edu.cn
Chunyan Yu,
✉ yuchunyan@szu.edu.cn

SPECIALTY SECTION

This article was submitted to Structural
Materials,
a section of the journal
Frontiers in Materials

RECEIVED 30 September 2022

ACCEPTED 07 February 2023

PUBLISHED 23 February 2023

CITATION

Liu W, Chen K and Yu C (2023), Grain-
boundary segregation and superior
mechanical properties in a
multicomponent L₁₂
Ni_{46.5}Co₂₄Fe₈Al_{12.5}Ti₉ superlattice alloy.
Front. Mater. 10:1058762.
doi: 10.3389/fmats.2023.1058762

COPYRIGHT

© 2023 Liu, Chen and Yu. This is an open-
access article distributed under the terms
of the [Creative Commons Attribution
License \(CC BY\)](https://creativecommons.org/licenses/by/4.0/). The use, distribution or
reproduction in other forums is
permitted, provided the original author(s)
and the copyright owner(s) are credited
and that the original publication in this
journal is cited, in accordance with
accepted academic practice. No use,
distribution or reproduction is permitted
which does not comply with these terms.

Grain-boundary segregation and superior mechanical properties in a multicomponent L₁₂ Ni_{46.5}Co₂₄Fe₈Al_{12.5}Ti₉ superlattice alloy

Weihong Liu^{1*}, Keyu Chen¹ and Chunyan Yu^{2*}

¹School of Materials Science and Engineering, Harbin Institute of Technology (Shenzhen), Shenzhen, China, ²College of Physics and Optoelectronic Engineering, Shenzhen University, Shenzhen, China

Ni₃Al superlattice alloys with the L₁₂ structure have garnered much attention due to their attractive high-temperature mechanical properties; however, their grain-boundary brittleness and low ductility in the ambient temperature range have greatly restricted their widespread application. In this study, we developed an L₁₂ structure multicomponent Ni_{46.5}Co₂₄Fe₈Al_{12.5}Ti₉ (at. %) superlattice alloy that notably suppressed the room-temperature intergranular brittleness and exhibited a large tensile elongation of 17.1% ± 5.2% together with a high ultimate tensile strength of 1,080.2 ± 57.4 MPa. Multiple microstructural examinations reveal an L₁₂ equiaxed-grain microstructure, with the presence of a minor B2 phase. Moreover, the co-segregation of Fe and Co atoms, and the associated reduction or elimination of the L₁₂ chemical order at the grain-boundary regions were characterized, which were proved to be the root cause of the suppression of intergranular brittleness and the high tensile ductility. Further theoretical calculations show that alloying of Fe and Co to binary Ni₃Al reduced the ordering energy, which promoted intergranular segregation and associated disordering. This observation demonstrated that the elimination or reduction of interfacial chemical order is an effective ductilizing method for superlattice alloys.

KEYWORDS

superlattice alloys, L₁₂ chemical order, grain-boundary brittleness, grain-boundary segregation, chemical disordering

1 Introduction

In the last century, great efforts have been devoted to the development of Ni₃Al superlattice alloys with the L₁₂ structure (Stoloff and Davies, 1968; Westbrook, 1977; Liu and Stiegler, 1984), which has been mostly ascribed to their anomalous yield behavior, relatively low densities, and good resistance to oxidation (Thorton et al., 1970; Liu and Roch, 1983; Pope and Ezz, 1984; George et al., 1994a). All these features are attractive factors for high-temperature applications. However, polycrystal Ni₃Al generally exhibits brittle intergranular fracture and poor ductility in the ambient temperature range (Grala et al., 1960; Liu et al., 1985; Povstugar et al., 2014). Therefore, grain boundaries (GBs) in strongly ordered L₁₂ Ni₃Al were considered to be more susceptible to fracture than their disordered face center cubic (fcc) solid solution counterparts. Despite this intrinsic factor, an extrinsic factor, namely, moisture-induced hydrogen embrittlement, was characterized to be the major cause of such brittle intergranular failure (George et al., 1994b; George et al., 1995).

Specifically, the embrittlement involves the reactive element Al decomposing H_2O in air ($2\text{Al} + 3\text{H}_2\text{O} \rightarrow \text{Al}_2\text{O}_3 + 6\text{H}$) to produce atomic hydrogen, which penetrates the tips of intergranular cracks, weakens atomic bonding, and hence promotes premature intergranular failure, known as environmental embrittlement (Liu et al., 1989; Stoloff and Liu, 1994). Such premature breakage prevents their use at any temperature and hence greatly restricts the widespread application of Ni_3Al as a high-temperature structural material.

Concentrated efforts have been devoted to improving the ductility of Ni_3Al , including micro-alloying, macro-alloying (Rawlings and Staton-Bevan, 1975; Liu et al., 1985; Aoki, 1990; Chiba et al., 1991; Chiba et al., 1992; Aoki et al., 1995), and grain-boundary engineering (Chiba et al., 1994; Cui et al., 2005). The most important discovery is that the intergranular brittleness can be suppressed by adding parts per million levels of boron, which segregates to GBs and modifies the properties of superlattice alloys. Subsequently, a tensile elongation of 50.8% and an ultimate tensile strength (UTS) of 1,315 MPa were observed in the Ni-enriched $\text{Ni}_{76}\text{Al}_{24}$ alloy upon testing in air (Liu et al., 1985; Aoki, 1990). Moreover, the tensile ductility of other polycrystalline L1_2 Ni_3Ge (Fang and Schulson, 1990), Ni_3Ga (Xu and Schulson, 1995), and Ni_3Si (Schulson et al., 1990) superlattice alloys was also improved by boron addition, which segregated to GBs and led to an enhanced resistance to intergranular brittleness. However, the yield strength (YS) of boron-doped binary Ni_3Al was still at a relatively low level of ~ 291 MPa (Liu et al., 1985), which is insufficiently strong for many engineering uses. Recently, Yang et al. (Yang et al., 2020) developed a boron-adopted multicomponent $\text{Ni}_{43.9}\text{Co}_{22.4}\text{Fe}_{8.8}\text{Al}_{10.7}\text{Ti}_{11.7}\text{B}_{2.5}$ (at. %) L1_2 alloy, which exhibited an excellent combination of a high YS of over 1 GPa and a tensile elongation of up to 28%. Multiscale analysis identified that boron addition induced co-segregation of boron, Fe, and Co atoms, and hence destroyed the local L1_2 order in the vicinity of GBs, which eliminated the intergranular brittleness, resulting in superior ductility. Similar to the ductilization of binary L1_2 Ni_3Al , the tensile ductility enhancement of the multicomponent $\text{Ni}_{43.9}\text{Co}_{22.4}\text{Fe}_{8.8}\text{Al}_{10.7}\text{Ti}_{11.7}\text{B}_{2.5}$ L1_2 alloy also strongly depends on boron addition, which blurs the understanding of the role of other alloying elements such as Fe, Co, and Ti on the origins of Fe and Co segregation.

In this study, we unprecedentedly developed a boron-free L1_2 -structured $\text{Ni}_{46.5}\text{Co}_{24}\text{Fe}_8\text{Al}_{12.5}\text{Ti}_9$ multicomponent alloy, which exhibits a tensile elongation as high as $\sim 17.1 \pm 5.2\%$ together with a high YS of 542.7 ± 4.0 MPa and an UTS of $1,080.2 \pm 57.4$ MPa. Careful microstructural examinations employing X-ray diffraction (XRD) and electron backscatter diffraction (EBSD) revealed an equiaxed-grain microstructure consisting of mainly the L1_2 phase and a small fraction of the B2 phase, with no major difference to that of binary Ni_3Al (Liu et al., 1985; Aoki, 1990). We further used high-resolution transmission electron microscopy (TEM) and aberration-corrected scanning TEM (STEM) equipped with energy dispersive X-ray spectroscopy (EDS) to examine the fine chemistry and structure at the grain-boundary regions. Co-segregation of Fe and Co and associated compositional disordering were characterized, which was identified to be the root cause of the ductility enhancement in the multicomponent $\text{Ni}_{46.5}\text{Co}_{24}\text{Fe}_8\text{Al}_{12.5}\text{Ti}_9$ L1_2 alloy. The atomistic

origin of the segregation was further discussed based on density functional theory (DFT) calculations. The findings presented here enable the development of high-performance superlattice alloys by controllable grain-boundary segregation.

2 Methods

2.1 Material preparation

The alloy with a nominal chemical composition of $\text{Ni}_{46.5}\text{Co}_{24}\text{Fe}_8\text{Al}_{12.5}\text{Ti}_9$ (at. %) was prepared from raw elements (~ 99.9 wt. % purity) by arc-melting under argon protection. The alloy ingots were re-melted four times by turning over to ensure chemical homogeneity and then, were drop-cast into a water-cooled copper mold with dimensions of $15 \times 3 \times 60$ mm. The obtained ingots were subsequently solution-treated at $1,050^\circ\text{C}$ for 1 h and were repeatedly cold-rolled (8% reduction per pass) to 1.5 mm-thick sheets, with intermediate annealing at $1,050^\circ\text{C}$ for 30 min. Intermediate treatments and the final recrystallization ($1,050^\circ\text{C}$ for 30 min) were carried out under a flowing argon atmosphere followed by air cooling to room temperature.

2.2 Microstructural characterization and mechanical testing

Crystal structure identification was performed using an X-ray diffractometer (Rigaku) with Cu K α radiation, scanning over the 2θ range 20° – 90° with a rate of $2^\circ/\text{min}$. Microstructural observations were conducted on a scanning electron microscope (SEM, Zeiss, Supra-55) and a field emission transmission electron microscope with selected area electron diffraction (SAED), operating at an accelerating voltage of 300 kV (JEM-3200FS). EBSD measurements were conducted on a field emission SEM (Zeiss, Supra-55) operating at an accelerating voltage of 20 kV, with a step size ranging between 0.3–1 μm . EDS analysis was conducted on a SEM (Zeiss, Supra-55) and an aberration-corrected scanning transmission electron microscope (Thermo Fisher Titan G260-300) to analyze the L1_2 and B2 phase compositions and the local chemical distribution across the boundary, respectively. To confirm data repeatability, three sets of data were collected and the standard deviation is included in Table 1.

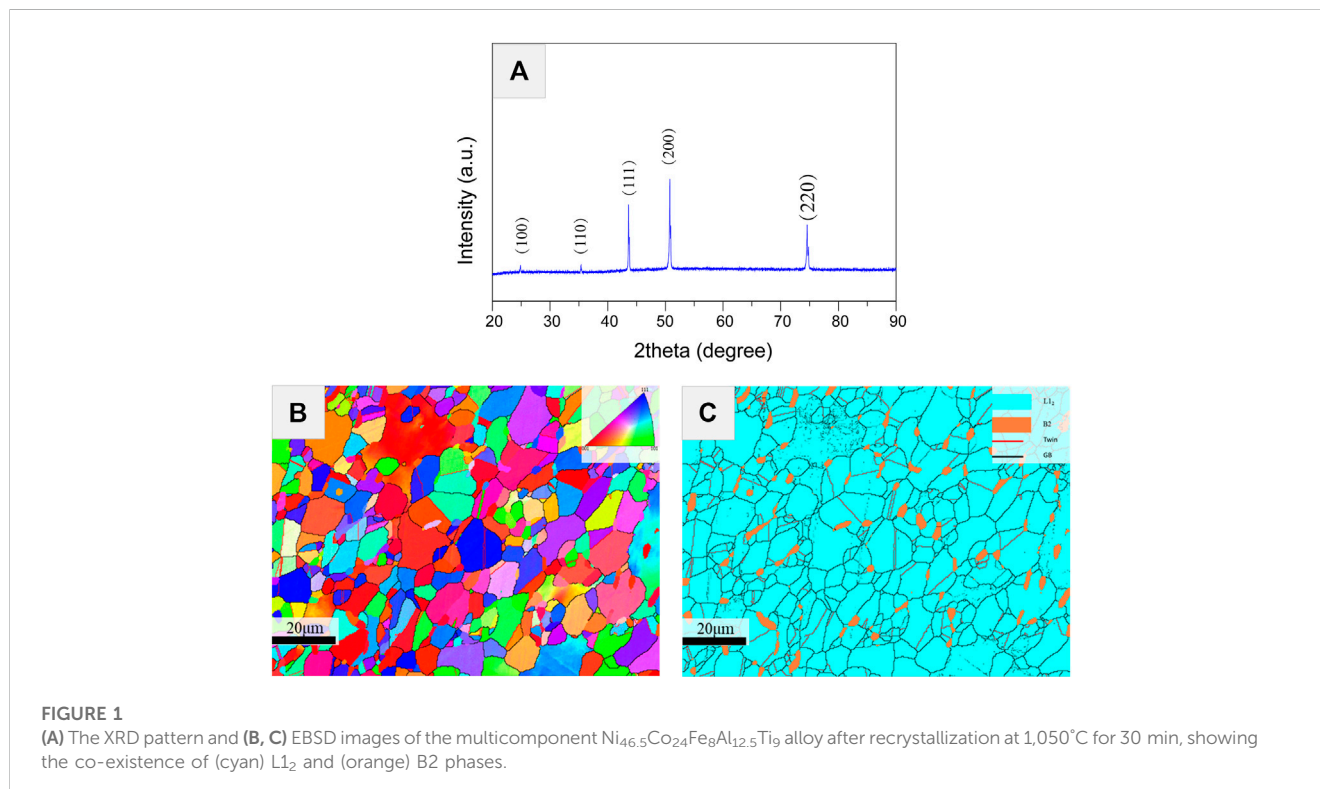
For EBSD observations, samples were cut from the recrystallized alloy before and after mechanical testing. These samples were first mechanically ground using 60–2000 μm SiC grinding papers, followed by carefully polishing using 20 nm colloidal silica for 30 min to obtain mirror-like and strain-free surfaces. The phase fraction was quantified as the area fraction measured from the EBSD phase map. Specimens for TEM and STEM observations were mechanically thinned to a thickness of approximately 100 μm , and then punched into 3 mm diameter discs. After that, samples were polished in a solution consisting of 10% perchloric acid and 90% alcohol at a temperature of -20°C using a Twin-Jet Electropolisher.

Dog-boned shaped tensile samples with a gauge section of $12.5 \times 1.5 \times 3$ mm were machined from the recrystallized alloy. Before testing, these tensile samples were ground to a 2000-grit finish by using SiC grinding papers. Uniaxial tensile tests were performed on a

TABLE 1 Phase composition of the $\text{Ni}_{46.5}\text{Co}_{24}\text{Fe}_8\text{Al}_{12.5}\text{Ti}_9$ alloy.

Phase	Chemical composition (at. %)				
	Ni	Co	Fe	Al	Ti
Bulk	46.5	24	8	12.5	9
$L1_2$	46.21 ± 0.27	24.42 ± 0.17	7.93 ± 0.01	13.07 ± 0.28	8.37 ± 0.16
B2	37.07 ± 0.03	20.39 ± 0.16	14.41 ± 0.36	21.76 ± 0.29	6.36 ± 0.05

Bold values are Standard deviation.



Material Testing System machine (Shimadzu) with a constant strain rate of $5 \times 10^{-4} \text{ s}^{-1}$ at room temperature in air, where a clip-on extensometer was used to attain the YS. At least three samples were tested to confirm data reproducibility. The fracture surfaces of these tested specimens were observed using a field-emission SEM (Zeiss, Supra-55).

2.3 First principles calculations

First principles calculations were conducted to understand the fundamental origins of Fe and Co segregation in the $\text{Ni}_{46.5}\text{Co}_{24}\text{Fe}_8\text{Al}_{12.5}\text{Ti}_9$ alloy. The formation energies of $L1_2$ and fcc structures for all the compositions were calculated by conducting first-principles calculations. Supercells with $4 \times 4 \times 3$ unit cells for each composition were generated by means of the special quasirandom structure method (Zunger et al., 1990). Spin-polarized calculations were performed using the Vienna *ab initio* Simulation Package (Kresse and Furthmüller, 1996) based on DFT.

The projector augmented wave (Blöchl, 1994) method with a cutoff energy of 500 eV was applied, and the electronic exchange and correlation were described by the generalized gradient approximation in the form of Perdew, Burke, and Ernzerhof (Perdew et al., 1996). The Brillouin zone was sampled by using the Gamma-centered Monkhorst–Pack scheme (Monkhorst and Pack, 1976) with $1 \times 1 \times 1$ k-points. Equilibrium cell volumes and all internal atomic positions of the supercells were optimized until convergence at a total energy tolerance of 10^{-4} eV.

3 Results

3.1 As-annealed microstructures

Figure 1A shows the XRD pattern of the $\text{Ni}_{46.5}\text{Co}_{24}\text{Fe}_8\text{Al}_{12.5}\text{Ti}_9$ alloy after recrystallization at $1,050^\circ\text{C}$ for 30 min. In addition to disordered reflection lines, ordered reflection lines at low angles of 24.8° and 35° , i.e., (001) and/or (011), corresponding to the $L1_2$

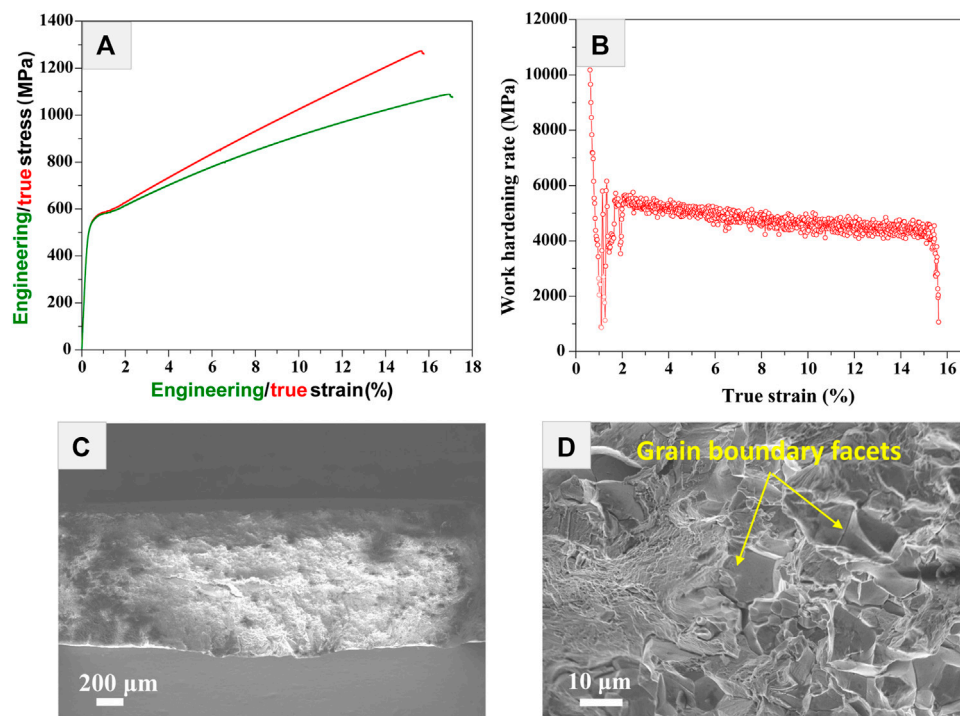


FIGURE 2
 (A) Engineering/true tensile stress-strain curves, (B) work hardening rate-strain curve, and (C, D) macroscopical and microscopical fracture surfaces of the multicomponent $\text{Ni}_{46.5}\text{Co}_{24}\text{Fe}_8\text{Al}_{12.5}\text{Ti}_9$ L_{12} alloy tested in air at room temperature.

structure, were observed. The observed L_{12} reflection lines were very sharp, indicating the well-established ordered structure and well-annealed microstructures. EBSD was employed to further examine the recrystallized alloy's microstructure. As shown in Figures 1B, C, the alloy exhibits an equiaxed-grain microstructure, with an average grain size of $8.5 \pm 3.2 \mu\text{m}$. Besides the expected L_{12} phase characterized by the XRD pattern, a small fraction of the B2 phase was identified in the EBSD measurement (Figure 1C). The alloy consists of the L_{12} phase (95.4%) and minor B2 phase (4.6%). Based on the EDS results in Table 1, the L_{12} phase composition is $\text{Ni}_{46.21}\text{Co}_{24.42}\text{Fe}_{7.93}\text{Al}_{13.07}\text{Ti}_{8.37}$, which is very close to the nominal chemical composition ($\text{Ni}_{46.5}\text{Co}_{24}\text{Fe}_8\text{Al}_{12.5}\text{Ti}_9$). The B2 phase composition is $\text{Ni}_{37.07}\text{Co}_{20.39}\text{Fe}_{14.41}\text{Al}_{21.76}\text{Ti}_{6.36}$. Based on the above analysis, there is no major microstructural difference between the L_{12} structured multicomponent $\text{Ni}_{46.5}\text{Co}_{24}\text{Fe}_8\text{Al}_{12.5}\text{Ti}_9$ and binary Ni_3Al (Liu et al., 1985; Aoki et al., 1995) alloys.

3.2 Room-temperature mechanical properties

Next, we measured the mechanical properties of the boron-free multicomponent L_{12} -structured $\text{Ni}_{46.5}\text{Co}_{24}\text{Fe}_8\text{Al}_{12.5}\text{Ti}_9$ alloy after recrystallization at $1,050^\circ\text{C}$ for 30 min. The representative engineering tensile stress-strain curve obtained at room temperature in air is presented in Figure 2A. Unprecedentedly, the multicomponent L_{12} alloy exhibits an elongation to fracture as high as $\sim 17.1 \pm 5.2\%$ together with a YS of 542.7 ± 4.0 MPa and an

UTS of $1,080.2 \pm 57.4$ MPa; a very competitive mechanical performance. It is impressive to observe such a high tensile elongation in a boron-free strongly L_{12} -ordered alloy, which is even comparable to the result of 25% for a 2.5 at % boron-adopted $\text{Ni}_{43.9}\text{Co}_{22.4}\text{Fe}_{8.8}\text{Al}_{10.7}\text{Ti}_{11.7}\text{B}_{2.5}$ alloy also with the L_{12} structure (Yang et al., 2020). To illustrate the designed alloy's work hardening capacity, the true strain-stress and -work hardening rate curves are shown in Figures 2A, B, respectively. Apparently, during the whole plastic deformation stage, the alloy has a very high work hardening capacity, which is consistent with boron-doped L_{12} Ni_3Al (Liu et al., 1985; Aoki, 1990).

The representative fracture surface is presented in Figures 2C, D. Macroscopically, less necking is observed (Figure 2C). Microscopically, the alloy fractured in a mixed transgranular and intergranular mode, with intergranular dominating, as shown in Figure 2D. These frequently observed smooth grain-boundary facets indicate that most GBs remain as weak links during tensile deformation. However, dimples were also occasionally observed, indicating that some GBs have a stronger resistance to fracture. Despite these intergranular fracture features, extensive plastic deformation was attained. Based on these observations, it was concluded that GBs in the multicomponent L_{12} alloy are not as intrinsically weak or brittle as those in binary L_{12} Ni_3Al (Liu et al., 1985; Aoki, 1990; Aoki et al., 1995). As stated previously, binary Ni_3Al fractured fully intergranularly, which resulted in poor tensile ductility at ambient temperature ranges^{13,14}. There is no major microstructure difference between our studied multicomponent alloy and binary Ni_3Al , except for the minor B2 phase in the

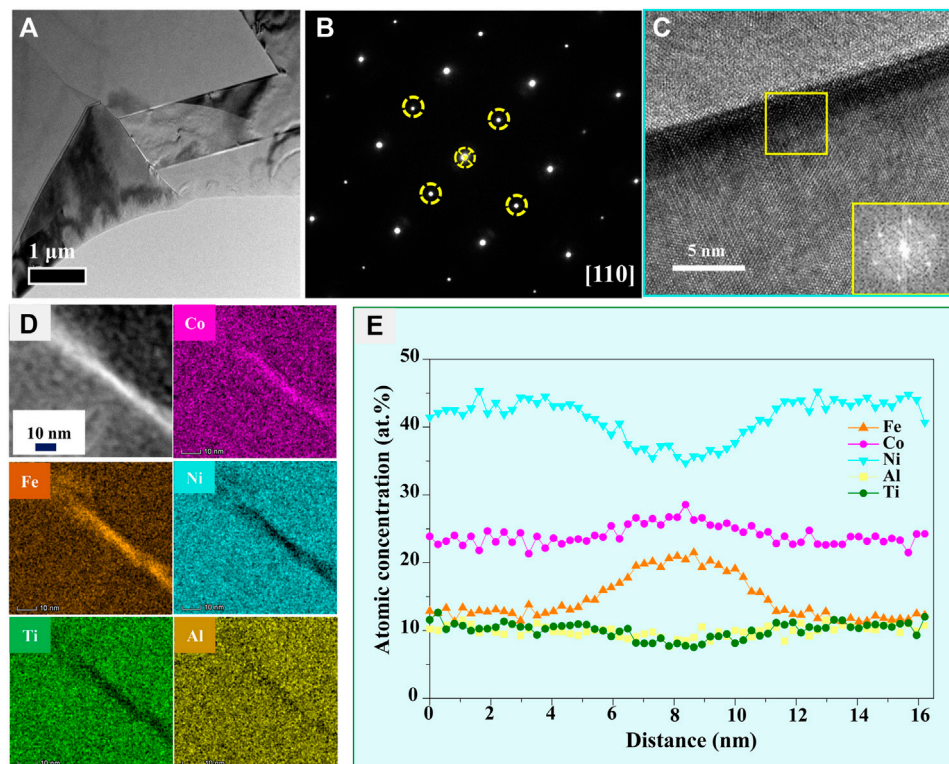


FIGURE 3

(A) Bright-field TEM image, (B) corresponding SEAD pattern, and (C) high-resolution TEM image of the $\text{Ni}_{46.5}\text{Co}_{24}\text{Fe}_8\text{Al}_{12.5}\text{Ti}_9$ alloy. The inset in (C) is the FFT pattern showing local disordering at the grain boundary region. (D) STEM-EDS mapping showing Fe and Co segregation at GBs and (E) corresponding compositional profiles across the boundary.

former. However, this phase has little influence on the mechanical properties due to its very low volume fraction and random distribution. Thus, the partial suppression of intergranular brittleness and the good tensile ductility of the multicomponent L_{12} alloy can be ascribed to their unique structures and the properties of GBs, which profoundly influence the mechanical properties of strongly L_{12} -ordered polycrystalline alloys.

3.3 Grain-boundary chemistry and structure

We next carefully examined the local chemistry and structure at grain-boundary regions in the multicomponent $\text{Ni}_{46.5}\text{Co}_{24}\text{Fe}_8\text{Al}_{12.5}\text{Ti}_9$ L_{12} alloy. The bright-field TEM image in Figure 3A shows polycrystalline morphologies without nanoscale clustering or precipitation along the GBs. The SAED patterns in Figure 3B present the L_{12} structure in the grain interiors, where two sets of spots were identified (marked by yellow circles). However, the high-resolution (HR) TEM image in Figure 3C shows local disordering in the close vicinity of GBs. Fast Fourier transformation (FFT) patterns further confirmed the chemically disordered fcc structure at the grain-boundary regions (see the inset of Figure 3C). Notably, we examined 3 GBs, and only two of them were found to have such local disordering, indicating that the degree of disordering was presumably associated with the grain-boundary character. To reveal the origins of interfacial disordering, STEM-

EDS mapping was employed to carefully examine the detailed compositional differences between granular and intergranular regions. As shown in Figure 3D, apparent Fe and Co segregation at GBs was observed, which was accompanied by depletions of Ni, Ti, and Al. For a detailed analysis, one-dimensional composition profiles across the boundary are presented in Figure 4E, revealing the segregation of Fe to ~22.4 at. %, 2.8 times the bulk concentration (8 at. %), and Co to ~27.5 at. %, approximately 14.6% higher than the bulk concentration (24 at. %). Meanwhile, Ni, Ti, and Al substantially depleted from 46.5 to 35 at. %, 9 to 7 at. %, and 12.5 to 7 at. %, respectively. The thickness of the segregation region was approximately 4 nm, which was the same as the disordered region in Figure 3C. Notably, three GBs were examined using STEM-EDS mapping, and different extents of segregation of Fe and Co at GBs were detected in all three. Such segregation could eliminate or reduce the L_{12} chemical order in the close vicinity of GBs, which enhances the resistance to intergranular failure in our designed multicomponent L_{12} alloy.

4 Discussion

Based on the above experimental results, it is evident that the mechanical properties of the L_{12} -structured $\text{Ni}_{46.5}\text{Co}_{24}\text{Fe}_8\text{Al}_{12.5}\text{Ti}_9$ alloy were strongly influenced by the extent of Fe and Co segregation and the associated partially/fully disordering at grain-boundary

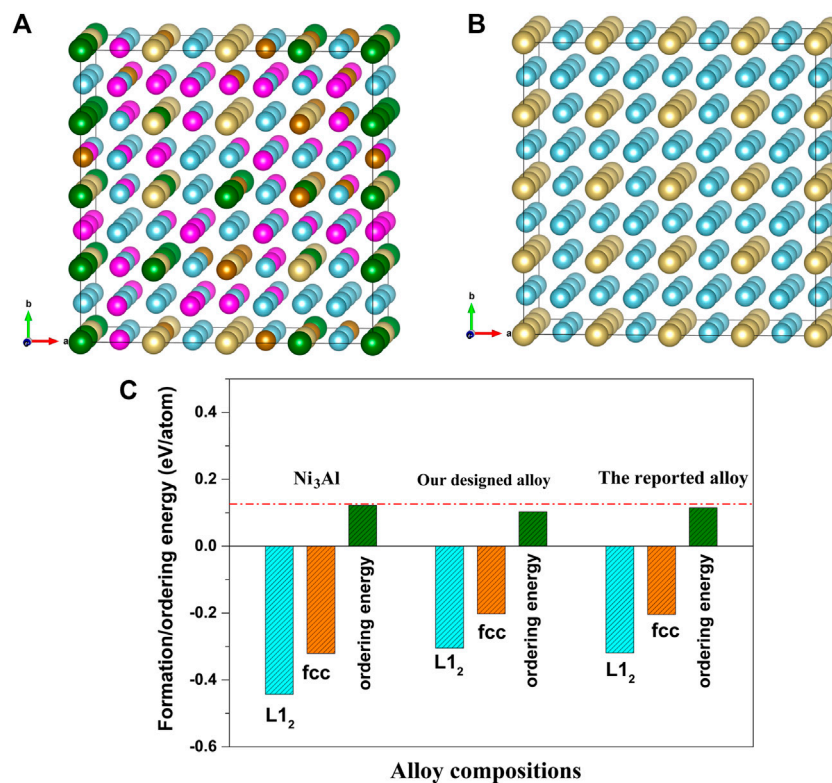


FIGURE 4

Supercell structures for the (A) multicomponent and (B) binary L₁₂ lattice determined by DFT calculations. (C) Calculated formation energies of the L₁₂ and fcc structures, as well as the corresponding ordering energy of Ni₃Al, our studied multicomponent L₁₂ alloy, and the previously reported Ni_{45.9}Co_{22.4}Fe_{8.8}Al_{10.7}Ti_{11.7}B_{0.5} L₁₂ alloy (Yang et al., 2020).

regions. On these grounds, two major fundamental issues need to be clarified: 1) why Fe and Co atoms segregate to GBs, and 2) why the localized Fe and Co segregation at GBs could improve the resistance against the intergranular fracture. This section will unveil the underlying mechanisms through combined theoretical and experimental studies.

4.1 Underlying mechanism for Co and Fe segregation

To start, co-segregation of Fe and Co at GBs in our designed Ni_{46.5}Co₂₄Fe₈Al_{12.5}Ti₉ L₁₂ alloy is certainly related to complex-site occupation in the L₁₂ lattice, which influences its formation energy, in particular the energy difference between the L₁₂ and fcc lattices, i.e., the ordering energy. Previously, Yang et al. (2020) revealed the site preference of Fe, Co, and Ti in another multicomponent L₁₂ Ni_{43.9}Co_{22.4}Fe_{8.8}Al_{10.7}Ti_{11.7}B_{2.5} alloy. The authors showed that Ti prefers Al sites, and in contrast, Co prefers Ni sites, while Fe tends to occupy both Ni and Al sites to sustain the stoichiometry of (Ni,Co,Fe)₃(Al,Ti,Fe). With these established elemental occupations, the supercell structure of (Ni,Co,Fe)₃(Al,Ti,Fe) was constructed from DFT calculations and is shown in Figure 4A. For comparison, the supercell structure of binary Ni₃Al was also constructed (Figure 4B). The formation energies of the L₁₂ and fcc structures for our designed Ni_{46.5}Co₂₄Fe₈Al_{12.5}Ti₉ alloy

were -0.305 and -0.202 eV/atom, respectively, as shown in Figure 4C. The ordering energy was determined to be 0.103 eV/atom (Figure 4C). The formation energies of the L₁₂ and fcc structures for the reported L₁₂ Ni_{45.9}Co_{22.4}Fe_{8.8}Al_{10.7}Ti_{11.7}B_{0.5} alloy composition (Yang et al., 2020), which was observed to have slight Fe and Co segregation, were also calculated. The values were -0.319 and -0.204 eV/atom, respectively, which were both a little lower than our designed alloy. More interestingly, its ordering energy of 0.115 eV/atom was larger than that calculated for our studied alloy: 0.103 eV/atom, as shown in Figure 4C. Another interesting fact is that the L₁₂ formation energies of the two multicomponent alloys were both much higher than -0.443 eV/atom for Ni₃Al, while their ordering energies were lower than 0.122 eV/atom for Ni₃Al, which has no elemental segregation at GBs (Liu et al., 1985), as shown in Figure 4C. These calculated results demonstrate that alloying Co, Fe, and Ti to binary Ni₃Al significantly increased the L₁₂ formation energy and reduced the ordering energy.

Then, we attempt to answer the following question: what are the individual effects of Fe, Co, and Ti on the ordering energy. First, Co and Fe atoms have been identified to be fcc formers for Ni₃Al (Chiba et al., 1992), and their incorporation should reduce the ordering energy. Furthermore, although the L₁₂ Ni₃Ti phase is thermodynamically unstable compared with the D0₂₄ structure, Ti has been identified to be a strong L₁₂ stabilizer for Ni₃Al (Kobayashi et al., 2012), and the incorporation of Ti should

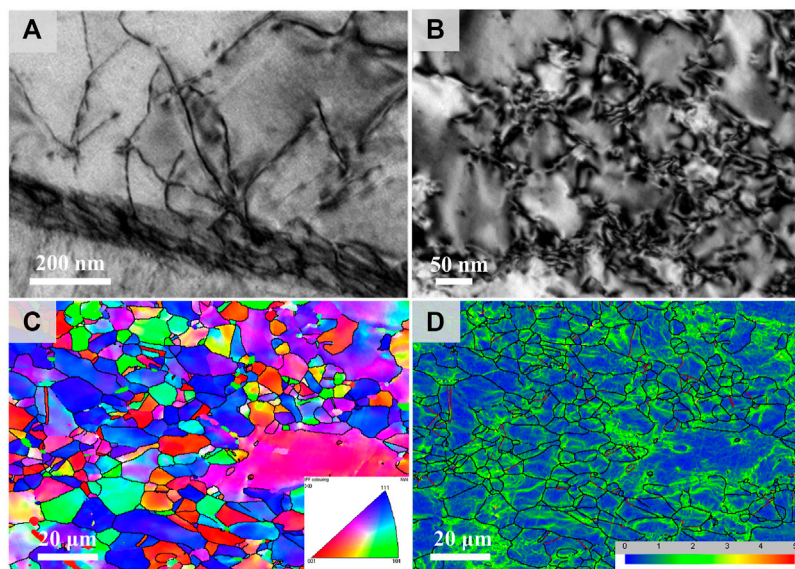


FIGURE 5
Bright-field TEM micrograph of the L₁₂ Ni_{46.5}Co₂₄Fe₈Al_{12.5}Ti₉ alloy after (A) 5% strain and (B) fracture. EBSD measurements of the fractured alloy (C, D).

increase the ordering energy. Therefore, it is expected that “foreign” Fe and Co atoms have the propensity to escape the imprisonment of neighboring atoms such as Al and/or Ti in the multicomponent L₁₂ lattice and segregate to loosely packed grain-boundary regions. Such segregation would lead to partially/fully disordering, depending on the extent of segregation, which is related to the ordering energy of the alloy compositions. We believe that the reduced ordering preference lowers the propensity to preserve the L₁₂ compositional order at the grain-boundary planes.

Importantly, compared with our designed Ni_{46.5}Co₂₄Fe₈Al_{12.5}Ti₉ alloy, only limited segregation of Fe and Co was detected in the Ni_{45.9}Co_{22.4}Fe_{8.8}Al_{10.7}Ti_{11.7}B_{0.5} alloy, which also exhibited the L₁₂ structure (Yang et al., 2020). Such a difference may be ascribed to differences in their ordering energies. As indicated in Figure 4C, the ordering energy of the Ni_{45.9}Co_{22.4}Fe_{8.8}Al_{10.7}Ti_{11.7}B_{0.5} alloy is 0.115 eV/atom, which is higher than that of our designed Ni_{46.5}Co₂₄Fe₈Al_{12.5}Ti₉ L₁₂ alloy, 0.103 eV/atom, due to the higher Ti concentration (11.7 at. % vs. 9 at. %) and the lower Co and Fe concentration (31.2 at. % vs. 32 at. %). Another important point is that no elemental segregation was detected in binary Ni₃Al, with a high ordering energy of 0.122 eV/atom. It should be noted that the extent of segregation can be enlarged by an increased boron concentration in the multicomponent L₁₂ (Ni,Co,Fe)₃(Al,Ti,Fe) alloy system; severe boron-induced Fe and Co atoms segregation was detected in the Ni_{43.9}Co_{22.4}Fe_{8.8}Al_{10.7}Ti_{11.7}B_{2.5} alloy at a higher boron concentration (Yang et al., 2020). Moreover, boron additions can also induce co-segregation of boron and Ni in binary Ni₃Al, which boosted the high tensile ductility to 50.8% (Liu et al., 1985; Aoki, 1990). Based on the above analysis, it is reasonable for us to conclude that the segregating propensity and ordering energy are closely inter-related; a smaller ordering energy generally indicates a larger propensity for segregation at the grain-boundary regions.

This finding enables further development of Ni₃Al-based superlattice alloys with superior mechanical properties.

4.2 The role of disordering in the deformation mechanism

To reveal the role of segregation-induced disordering on plastic deformation, systematic EBSD mapping and TEM observations were conducted on the deformed Ni_{46.5}Co₂₄Fe₈Al_{12.5}Ti₉ alloy, interrupted at 5% and after fracture. As shown in Figure 5A, even at a low strain, massive dislocation pileups ahead of GBs were observed. At a high strain (~17.1%), dipoles and bundles of dipoles are characteristic features of the dislocation structure (Figure 5B). EBSD measurements on the fracture alloy reveal an apparent grain rotation and elongation along the tensile direction, as shown in Figure 5C, D. Moreover, evident geometry-necessary dislocation concentrations at GBs were detected. As shown in Figure 2D, most boundaries fractured at a strain of ~17.1%; however, there is still a small fraction of GBs fracturing transgranularly, indicating that the local stress concentration at these boundaries is not large enough to trigger intergranular cracks. These observations indicate that GBs in our designed Ni_{46.5}Co₂₄Fe₈Al_{12.5}Ti₉ L₁₂ alloy have stronger resistance to fracture than that for binary Ni₃Al without segregation and interfacial disordering. Moreover, it was reported that the L₁₂-structured Ni_{45.9}Co_{22.4}Fe_{8.8}Al_{10.7}Ti_{11.7}B_{0.5} alloy, which has limited Fe and Co segregation and no interfacial disordering (Yang et al., 2020), fractured fully intergranularly without any plastic deformation. A higher boron concentration in the Ni_{43.9}Co_{22.4}Fe_{8.8}Al_{10.7}Ti_{11.7}B_{2.5} L₁₂ alloy, which has Fe and Co segregation-induced chemical disordering at grain-boundary regions, made it fracture fully intergranularly and exhibit a high tensile elongation of 25% (Yang et al., 2020). Based on these facts, the resistance to intergranular fracture in the

multicomponent $L1_2$ (Ni,Co,Fe)₃(Al,Ti,Fe) alloy system is directly related to the extent of Co and Fe atom segregation and the associated chemical disordering at grain-boundary regions, which probably improved the cohesive strength of GBs and/or reduced the stress concentration at GBs.

On the one hand, it was considered that the cohesive strength of metallic materials influenced their fracture modes; however, theoretical calculations indicate that no distinct difference in boundary cohesive strength was identified between disordered Ni and ordered Ni₃Al (Chen et al., 1986; Vitek and Chen, 1991). On the other hand, atomistic studies have demonstrated that the intrinsic brittleness of GBs in Ni₃Al is mainly related to the full preservation of compositional order at GBs. Theoretically, Vitek and Chen (Vitek and Chen, 1991) have shown that the preservation of $L1_2$ chemical order at the boundary plane leads to the presence of atomic-sized holes, which can act as crack nucleation sites and promote intergranular failure. Moreover, such full preservation of chemical order also raises difficulties in slip transmission across GBs, since this requires the creation of anti-phase boundaries with a high energy. Based on the above analysis, it was concluded that the intergranular brittleness of strongly ordered $L1_2$ alloys is indeed directly related to the preservation of $L1_2$ chemical order at the GBs. If the chemical order would be destroyed by the co-segregation of Co and Fe atoms, this would not only remove atomic-sized cavities, but also make slip transmission across GBs easier, thereby reducing the likelihood of crack nucleation and suppressing intergranular fracture.

5 Conclusion

We have developed a multicomponent $L1_2$ -structured Ni_{46.5}Co₂₄Fe₈Al_{12.5}Ti₉ superlattice alloy, which has a large tensile elongation of $\sim 17.1 \pm 5.2\%$ together with a high YS of 542.7 ± 4.0 MPa and an UTS of $1,080.2 \pm 57.4$ MPa. SEM and EBSD measurements reveal that it has an equiaxed fine-grain microstructure mainly consisting of the $L1_2$ phase and a minor B2 phase. However, detailed TEM and STEM-EDS examination on the local microstructure at GBs reveals co-segregation of Fe and Co and partial/full interfacial disordering at grain-boundary regions, which serves as an effective and necessary requirement for overcoming intergranular brittleness. DFT calculations indicate that the incorporation of Fe and Co in binary Ni₃Al reduces the $L1_2$ ordering propensity, which promotes Fe and Co segregation and hence reduces or eliminates the $L1_2$ order degree at the grain-boundary region. These observations provide an effective method to design strong and ductile superlattice alloys by controllable grain-boundary segregation.

References

- Aoki, K. (1990). Ductilization of $L1_2$ intermetallic compound Ni₃Al by Microalloying with Boron. *Mater. Trans. JIM* 31 (6), 443–448. doi:10.2320/matertrans1989.31.443
- Aoki, K., Ishikawa, K., and Masumoto, T. (1995). Ductilization of Ni₃Al by alloying with boron and substitutional elements. *Mater. Sci. Eng. A* 192, 316–323. doi:10.1016/0921-5093(94)03213-0
- Blöchl, P. E. (1994). Projector augmented-wave method. *Phys. Rev. B* 50 (24), 17953–17979. doi:10.1103/physrevb.50.17953
- Chen, S., Voter, A., and Srolovitz, D. (1986). Computer simulation of grain boundaries in Ni₃Al: The effect of grain boundary composition. *Scr. Metall.* 20 (10), 1389–1394. doi:10.1016/0036-9748(86)90102-x
- Chiba, A., Hanada, S., Watanabe, S., Abe, T., and Obana, T. (1994). Relation between ductility and grain boundary character distributions in Ni₃Al. *Acta Metallurgica Materialia* 42 (5), 1733–1738. doi:10.1016/0956-7151(94)90383-2
- Chiba, A., Hanada, S., and Watanabe, S. (1991). Effect of γ and γ' former doping on ductility of Ni₃Al. *Scripta Metallurgica Materialia* 25 (2), 303–307. doi:10.1016/0956-716x(91)90183-2
- Chiba, A., Hanada, S., and Watanabe, S. (1992). "Improvement in ductility of Ni₃Al by γ former doping," in Proceedings of the Second International ASM Conference on High Temperature Aluminides and Intermetallics, San Diego, CA, USA, September 16–19, 108–113.

Data availability statement

The original contributions presented in the study are included in the article/supplementary material, further inquiries can be directed to the corresponding authors.

Author contributions

WL and CY conceived and supervised the research. KC and WL performed the experimental work. CY conducted the theoretical calculations. WL and CY analyzed the data and wrote the manuscript. All authors discussed the results and contributed to the final manuscript.

Funding

This research was supported by the National Natural Science Foundation of China (no. 5210010578), the Natural Science Foundation of Guangdong Province (no. 2022A1515011490), and the Natural Science Foundation of Shenzhen City (no. JCYJ20210324124007021).

Acknowledgments

We thank Q. Z. L. from the Southern University of Science and Technology for technical assistance with STEM-EDS.

Conflict of interest

The authors declare that the research was conducted in the absence of any commercial or financial relationships that could be construed as a potential conflict of interest.

Publisher's note

All claims expressed in this article are solely those of the authors and do not necessarily represent those of their affiliated organizations, or those of the publisher, the editors and the reviewers. Any product that may be evaluated in this article, or claim that may be made by its manufacturer, is not guaranteed or endorsed by the publisher.

- Cui, C., Demura, M., Kishida, K., and Hirano, T. (2005). Ductility of cold-rolled and recrystallized Ni3Al foils. *J. Mater. Res.* 20 (4), 1054–1062. doi:10.1557/jmr.2005.0142
- Fang, J., and Schulson, E. (1990). Preliminary indications of a slight improvement in the ductility of Ni3Ge with boron. *MRS Online Proc. Libr. Opl.* 213, 751. doi:10.1557/proc-213-751
- George, E., Liu, C., Lin, H., and Pope, D. (1995). Environmental embrittlement and other causes of brittle grain boundary fracture in Ni3Al. *Mater. Sci. Eng. A* 192, 277–288. doi:10.1016/0921-5093(94)03236-x
- George, E., Liu, C., and Pope, D. (1994). Effect of vacuum on room-temperature ductility of Ni3Al. *United States* 30 (1), 37–42. doi:10.1016/0956-716x(94)90354-9
- George, E., Yamaguchi, M., Kumar, K., and Liu, C. (1994). Ordered intermetallics. *Annu. Rev. Mater. Sci.* 24 (1), 409–451. doi:10.1146/annurev.ms.24.080194.002205
- Grala, E., and Westbrook, J. (1960). in *Mechanical properties of intermetallic compounds*. Editor J. H. Westbrook (New York: John Wiley), 358.
- Kobayashi, S., Sato, K., Hayashi, E., Osaka, T., Konno, T. J., Kaneno, Y., et al. (2012). Alloying effects on the phase equilibria among Ni (A1), Ni3Al (L12) and Ni3V (D022) phases. *Intermetallics* 23, 68–75. doi:10.1016/j.intermet.2011.12.008
- Kresse, G., and Furthmüller, J. (1996). Efficient iterative schemes for *ab initio* total-energy calculations using a plane-wave basis set. *Phys. Rev. B* 54 (16), 11169–11186. doi:10.1103/physrevb.54.11169
- Liu, C., Lee, E., and McKamey, C. (1989). An environmental effect as the major cause for room-temperature embrittlement in FeAl. *Scr. Metall.* 23 (6), 875–880. doi:10.1016/0036-9748(89)90263-9
- Liu, C., and Roch, C. (1983). *Development of ductile polycrystalline Ni3Al for high-temperature applications* Technical Aspects of Critical Materials Use by the Steel Industry 1, 83–2672.
- Liu, C., and Stiegler, J. (1984). Ductile ordered intermetallic alloys. *Science* 226 (4675), 636–642. doi:10.1126/science.226.4675.636
- Liu, C. T., White, C., and Horton, J. (1985). Effect of boron on grain-boundaries in Ni3Al. *Acta metall.* 33 (2), 213–229. doi:10.1016/0001-6160(85)90139-7
- Monkhorst, H. J., and Pack, J. D. (1976). Special points for Brillouin-zone integrations. *Phys. Rev. B* 13 (12), 5188–5192. doi:10.1103/physrevb.13.5188
- Perdew, J. P., Burke, K., and Ernzerhof, M. (1996). Generalized gradient approximation made simple. *Phys. Rev. Lett.* 77 (18), 3865–3868. doi:10.1103/physrevlett.77.3865
- Pope, D., and Ezz, S. S. (1984). Mechanical properties of Ni3Al and nickel-base alloys with high volume fraction of γ . *Int. Met. Rev.* 29 (1), 136–167. doi:10.1179/imtr.1984.29.1.136
- Povstugar, I., Choi, P.-P., Neumeier, S., Bauer, A., Zenk, C. H., Göken, M., et al. (2014). Elemental partitioning and mechanical properties of Ti- and Ta-containing Co–Al–W-base superalloys studied by atom probe tomography and nanoindentation. *Acta Mater.* 78, 78–85. doi:10.1016/j.actamat.2014.06.020
- Rawlings, R. D., and Staton-Bevan, A. E. (1975). The alloying behaviour and mechanical properties of polycrystalline Ni3Al (γ' phase) with ternary additions. *J. Mater. Sci.* 10 (3), 505–514. doi:10.1007/bf00543696
- Schulson, E., Briggs, L., and Baker, I. (1990). The strength and ductility of Ni3Si. *Acta Metallurgica Materialia* 38 (2), 207–213. doi:10.1016/0956-7151(90)90050-q
- Stoloff, N. S., and Davies, R. G. (1968). The mechanical properties of ordered alloys. *Prog. Mater. Sci.* 13, 1–84. doi:10.1016/0079-6425(68)90018-2
- Stoloff, N. S., and Liu, C. (1994). Environmental embrittlement of iron aluminides. *Intermetallics* 2 (2), 75–87. doi:10.1016/0966-9795(94)90001-9
- Thorton, P., Davies, R., and Johnston, T. (1970). The temperature dependence of the flow stress of the γ' Phase based upon Ni 3 Al. *Metall. Trans.* 1, 207–218.
- Vitek, V., and Chen, S. (1991). Modeling of grain boundary structures and properties in intermetallic compounds. *Scr. Metallurgica;(United States)* 25 (6), 1237–1242. doi:10.1016/0956-716x(91)90393-f
- Westbrook, J. H. (1977). Intermetallic compounds: Their past and promise. *Metall. Trans. A* 8 (9), 1327–1360. doi:10.1007/bf02642848
- Xu, Y., and Schulson, E. (1995). Strength and ductility of Ni3Ga with and without boron. *Acta metallurgica materialia* 43 (5), 2121–2132. doi:10.1016/0956-7151(94)00394-w
- Yang, T., Zhao, Y., Li, W., Yu, C., Luan, J., Lin, D., et al. (2020). Ultrahigh-strength and ductile superlattice alloys with nanoscale disordered interfaces. *Science* 369 (6502), 427–432. doi:10.1126/science.abb6830
- Zunger, A., Wei, S.-H., Ferreira, L., and Bernard, J. E. (1990). Special quasirandom structures. *Phys. Rev. Lett.* 65 (3), 353–356. doi:10.1103/physrevlett.65.353